creative commons
COMMONS DEED

저작자표시-비영리-변경금지 2.0 대한민국

이용자는 아래의 조건을 따르는 경우에 한하여 자유롭게

- 이 저작물을 복제, 배포, 전송, 전시, 공연 및 방송할 수 있습니다.

다음과 같은 조건을 따라야 합니다:

저작자표시. 귀하는 원저작자를 표시하여야 합니다.

비영리. 귀하는 이 저작물을 영리 목적으로 이용할 수 없습니다.

변경금지. 귀하는 이 저작물을 개작, 변형 또는 가공할 수 없습니다.

- 귀하는, 이 저작물의 재이용이나 배포의 경우, 이 저작물에 적용된 이용허락조건을 명확하게 나타내어야 합니다.
- 저작권자로부터 별도의 허가를 받으면 이러한 조건들은 적용되지 않습니다.

저작권법에 따른 이용자의 권리는 위의 내용에 의하여 영향을 받지 않습니다.

이것은 이용허락규약(Legal Code)을 이해하기 쉽게 요약한 것입니다.

Disclaimer

dCollection

연세대학교
YONSEI UNIVERSITY

Discovery of predictive biomarkers for oncolytic virus therapy in metastatic renal cell carcinoma

Won Sik Jang

Department of Medicine

The Graduate School, Yonsei University

연세대학교
YONSEI UNIVERSITY

Discovery of predictive biomarkers for oncolytic virus therapy in metastatic renal cell carcinoma

Directed by Professor Won Sik Ham

The Doctoral Dissertation
submitted to the Department of Medicine,
the Graduate School of Yonsei University
in partial fulfillment of the requirements for the degree of
Doctor of Philosophy in Medical Science

Won Sik Jang

December 2022

연세대학교
YONSEI UNIVERSITY

This certifies that the Doctoral Dissertation of
Won Sik Jang is approved.

Thesis Supervisor : Won Sik Ham

Thesis Committee Member#1 : Woong Sub Koom

Thesis Committee Member#2 : Sang Joon Shin

Thesis Committee Member#3 : Jae Moon Yang

Thesis Committee Member#4 : Serk In Park

The Graduate School
Yonsei University

December 2022

연세대학교
YONSEI UNIVERSITY

ACKNOWLEDGEMENTS

First of all, I would like to thank my supervisor, Prof. Won Sik Ham as my mentor who has been most supportive to me finishing my Ph.D study. His advice and guidance have always been great encouragement for me.

Besides my supervisor, I also appreciate the rest of my thesis committee: Prof. Woong Sub Koom, Sang Joon Shin, Jae Moon Yang, and Serk In Park who gave me expert advice.

My sincere thanks also go to Dr. Jee Soo Park. Without his help, it really would have been difficult for me to complete this research. I am deeply grateful for his support.

I thank members of our lab: PhD. Myung Eun Lee and Se Mi Park for their assistance and supports.

Last but not the least, I thank my family from the bottom of my heart for great their support and love being with me always.

연세대학교
YONSEI UNIVERSITY

<TABLE OF CONTENTS>

연세대학교
YONSEI UNIVERSITY

연세대학교
YONSEI UNIVERSITY

LIST OF FIGURES

연세대학교
YONSEI UNIVERSITY

LIST OF TABLES

연세대학교
YONSEI UNIVERSITY

ABSTRACT

Discovery of predictive biomarkers for oncolytic virus therapy in metastatic renal cell carcinoma

Won Sik Jang

Department of Medicine
The Graduate School, Yonsei University

(Directed by Professor Won Sik Ham)

Background:

Immune checkpoint inhibitors and tyrosine kinase inhibitors are the first-line treatment for metastatic renal cell carcinoma (mRCC), but their benefits are limited to specific patient subsets. JX-594 (pexastimogene devacirepvec, Pexa-vec) is a thymidine kinase-deleted oncolytic vaccinia virus and has been engineered to express granulocyte macrophage-colony stimulating factor (GM-CSF), an immune-activating transgene. JX-594 possesses anticancer activity with low toxicity, as reported in preclinical and clinical studies. We aimed to evaluate the therapeutic efficacy of JX-594 monotherapy by systemic injection in metastatic orthotopic RCC murine models. Furthermore, we investigated and compared the therapeutic efficacy of JX-594 according to the four most commonly mutated genes (*VHL*, *PBRM1*, *SETD2*, and *BAP1*) in ccRCC, suggesting the potential predictive biomarkers of JX-594.

Methods:

Two highly metastatic orthotopic RCC models were developed to compare the treatment efficacy in the International Metastatic RCC Database Consortium favorable-risk and intermediate- or poor-risk groups. JX-594 was systemically injected through the peritoneum, whereas sunitinib was orally administered. Post-treatment, tumor

연세대학교
YONSEI UNIVERSITY

microenvironment (TME) remodeling was determined using immunofluorescence analysis. Four cell-line derived xenograft (CDX) mouse models have been developed using the ccRCC cell lines representative of each four mutations (786-O (*VHL* mutation), Caki-2 (*VHL* and *PBRM1* mutation), A-498 (*VHL* and *SETD2* mutation), and 769-P (*VHL* and *BAP1* mutation)). Tumors were implanted by subcutaneous injection into the right flank of wild-type BALB/c nude mice. JX-594 by intratumoral injection in day 0, 3, and 6. Tumor volume was calculated with digital calipers every 3 days. Tumor growth rate was calculated by the increased tumor volume divided by the day which was measured between day 0 and 12. Relative therapeutic response ratio was calculated in order to adjust the relative differences in tumor growth rate of each cell line and compare the actual therapeutic effects of JX-594 in each cell line. mRNA expressions of interferon beta (IFN-β) were measured with qRT-PCR after the JX-594 treatment in786-O, Caki-2, A-498 and 769-P in order to validate the hypoxia-inducible factor (HIF)-dependent IFN-β pathway.

Results:

Systemic JX-594 monotherapy injection demonstrated therapeutic benefit in both early- and advanced-stage mRCC models. Sunitinib monotherapy significantly reduced the primary tumor burden and number of lung metastases in the early-stage, but not in the advanced-stage mRCC model. Systemic JX-594 delivery remodeled the primary TME and lung metastatic sites by increasing tumor-infiltrating CD4/8+ T cells and dendritic cells. Systemic JX-594 monotherapy demonstrated significantly better therapeutic outcomes compared with sunitinib monotherapy in both early- and advanced-stage mRCCs by converting cold tumors into hot tumors. All four CDX models demonstrated significant decrease in tumor size by the JX-594 treatment compared to control. Most rapid tumor growth was noted at *BAP1* mutation tumors while *PBRM1* mutation tumor demonstrated the slowest growth. The decrease of tumor volume was most significant in *BAP1* mutation tumors compared to tumors with *VHL*, *PBRM1*, and *SETD2* mutations. In terms of relative therapeutic response ratio which adjusted the relative difference in a tumor growth rate of

연세대학교
YONSEI UNIVERSITY

each cell line, *BAP1* mutation was also associated with a better relative therapeutic response ratio. Meanwhile, IFN-β mRNA expression was significantly decreased in *BAP1*-deficient cell line compared to other cell lines, while the expression level was recovered dramatically after JX-594.

Conclusions:

The systemic injection of JX-594 dynamically remodeled the TMEs from those of cold to those of hot tumors and activated anti-cancer immunity, which suppressed both the primary tumors and the lung metastases in early- and advanced-stage mRCCs. Sunitinib has limited efficacy in early-stage mRCC, but its role in improving the immunotherapeutic outcomes should be further investigated. *BAP1* demonstrated its potential for predictive biomarker for JX-594 treatment. Our study is the first to provide the findings that JX-594 monotherapy could be considered as the treatment option for mRCC and *BAP1* could be used as the guidance for the use of JX-594 although future clinical studies are needed.

Key words : immunotherapy; oncolytic virus; renal cell carcinoma; tumor microenvironment; biomarker

연세대학교
YONSEI UNIVERSITY

Discovery of predictive biomarkers for oncolytic virus therapy in metastatic renal cell carcinoma

Won Sik Jang

Department of Medicine
The Graduate School, Yonsei University

(Directed by Professor Won Sik Ham)

I. INTRODUCTION

Approximately one-third of all patients diagnosed with renal cell carcinoma (RCC) already have systemic diseases at the time of the first diagnosis.[1] Although significant improvements in the therapeutic strategies for metastatic RCC (mRCC) have been achieved, the five-year survival rate is less than 10%, with incidence and mortality rates rising at a rate of 2–3% per decade.[2] mRCC remains a significant health issue as it is an incurable disease.[3] In the last decade, sunitinib (Sutent; Pfizer, NY, USA), a multikinase inhibitor with antiangiogenic properties, has developed into a standard first-line treatment option for advanced mRCC.[4] However, cancer immunotherapy, particularly with immune checkpoint inhibitors (ICIs), has recently emerged as a potent and effective therapeutic strategy for advanced cancers, replacing sunitinib.[5,6] CheckMate 214 demonstrated the superiority of nivolumab and ipilimumab over sunitinib in patients with intermediate- and poor-risk disease.[7] After this study, immuno-oncology (IO) agents have changed the treatment paradigm for mRCC as IO combination therapies have now become the first-line therapy for mRCC.[8]

Antibodies targeting immune checkpoints, such as cytotoxic T-lymphocyte associated protein-4, programmed cell death protein 1 (PD-1), and programmed death-ligand (PD-L1), demonstrate anti-tumor effects in various malignancies. However, ICI efficacy is limited in certain circumstances, deriving benefits for only a subset of patients. There is also a risk

연세대학교
YONSEI UNIVERSITY

of primary refractory status and subsequent resistance and recurrence after IO combination therapies.[9] Moreover, IO combination therapy has no clear advantage over vascular endothelial growth factor receptor-tyrosine kinase inhibitors in the International Metastatic Renal Cell Carcinoma Database Consortium (IMDC) favorable risk group.[7,10,11]

The efficacy of ICIs is limited in the treatment of patients with advanced mRCC, with only 20–30% of patients responding to ICI monotherapy and others showing intrinsic resistance to ICI treatment due to a non-inflamed "cold" tumor microenvironment (TME).[12] Thus, novel immunotherapeutic agents are warranted to overcome this limitation by changing the TME through the depletion of cancer-promoting microenvironmental cells and their reeducation toward immune-stimulating, tumor-suppressive phenotypes.[13] This strategy is now widely appreciated as an anticancer armamentarium.[14] Oncolytic virus (OV) is one of the most promising treatment strategies for solid malignancies because it can remodel the TME toward a T cell-inflamed phenotype by stimulating host immune responses against the tumor.[12,15]

JX-594 (pexastimogene devacirepvec, Pexa-vec) is a thymidine kinase-deleted oncolytic vaccinia virus and has been engineered to express granulocyte macrophage-colony stimulating factor (GM-CSF), an immune-activating transgene.[16,17] JX-594 possesses anticancer activity with low toxicity, as reported in preclinical and clinical studies.[17] Numerous clinical trials showed that JX-594 is one of the most feasible and promising OV platforms, along with a few OVs.[16-19] A few studies have demonstrated the immune-modulatory functions in the primary site of the TME after the intratumoral injection of JX-594.[17] However, no studies have evaluated the therapeutic effects of JX-594 after its systemic injection in mRCC settings.

Despite the significant therapeutic advances for mRCC, including targeted therapies and ICIs, no specific biomarkers exist in routine clinical care that could facilitate the decision-making process by optimizing the sequence of current regimens.[20] Furthermore, no studies that have investigated the genetic biomarkers for JX-594. Integration of genetic mutation into treatment decision-making could personalize treatment strategies.[20] Several recent studies have reported clinical outcomes associated with treatment regimens according to the commonly mutated genes in clear cell RCC (ccRCC). In terms of antiangiogenic therapies, mutations in *PBRM1* demonstrated favorable response to antiangiogenic

연세대학교
YONSEI UNIVERSITY

therapies.[21,22] On the other hand, *BAP1* mutation has been associated with poor response to antiangiogenic therapies. For ICIs, *PBRM1* has been reported to be a potential predictive biomarker for ICI response. Loss-of-function in *PBRM1* was associated with significant clinical benefit for anti-PD-1 agent in the largest cohort database of CheckMate 009, 010, and 025.[23] Moreover, sarcomatoid/rhabdoid features in RCC have also been reported to be a potential surrogate marker for ICI response.[24]

In this study, we aimed to evaluate the therapeutic efficacy of JX-594 monotherapy via systemic injection in comparison with sunitinib monotherapy in metastatic orthotopic RCC murine models. We developed two different models among metastatic orthotopic RCC murine models to compare the therapeutic efficacy according to different IMDC risk groups (favorable vs. intermediate or poor). Furthermore, we have demonstrated the dynamic remodeling of the TME in the primary tumor site as well as distant metastatic sites after systemic treatment with JX-594. Lastly, we have evaluated and compared the therapeutic efficacy of JX-594 according to the four most commonly mutated genes (*VHL, PBRM1, SETD2,* and *BAP1*) in ccRCC,[25] suggesting the potential predictive biomarkers of JX-594 in addition to the explanation of possible molecular pathogenesis.

II. METHODS

1. RCC Cell Lines

Four human RCC cell lines which consist of 786-O (cat# CRL-1932), Caki-1 (cat# HTB-46), A-498 (cat# HTB-44), ACHN (cat# CRL-1611), and Renca, the murine RCC cell line, were purchased from the American Type Culture Collection (Manassas, VA, USA). Roswell Park Memorial Institute 1640 medium or Eagle's minimum essential medium in addition of 10% fetal bovine serum (Gibco; Thermo Fisher Scientific, Waltham, MA, USA) and 1% penicillin–streptomycin (Sigma-Aldrich, St. Louis, MO, USA) was used to culture cells (37 ℃ in a humidified atmosphere containing 5% CO_2).

For the study for development of predictive biomarkers for JX-594 therapy according to the four most commonly mutated genes (*VHL, PBRM1, SETD2,* and *BAP1*), 786-O, Caki-2, A-498 and 769-P were chosen. 786-O (cat# CRL-1932) represents ccRCC with *VHL*

연세대학교
YONSEI UNIVERSITY

mutation and Caki-2 (cat# HTB-47) represents ccRCC with *VHL* and *PBRM1* mutation. A-498 (cat# HTB-44) represents ccRCC with *VHL* and *SETD2* mutation and 769-P (cat# CRL-1933) represents ccRCC with *VHL* and *BAP1* mutation.[26]

2. Treatment Regimens

JX-594 and a mouse variant of JX-594 (mJX-594) were provided by SillaJen, Inc. (Seoul, Korea). JX-594 is a Wyeth strain vaccinia virus modified by insertion of the human GM-CSF and Lac-Z genes into the vaccinia thymidine kinase gene region under the control of the synthetic early/late and p7.5 promoters, respectively.[27] mJX-594 is a Western Reserve strain of vaccinia virus encoding murine GM-CSF in the vaccina thymidine kinase gene locus under the control of the p7.5 promoter.[28] The virus was stored at −80 °C. The anticancer drug sunitinib was purchased from Selleckchem (Houston, TX, USA).

3. Cell Proliferation (Cytotoxicity) Assay

Cells were seeded in 96-well culture plates at a density of 1×10^4 cells per well. The next day, the cells were treated with JX-594 or mJX-594 at the desired concentration in culture media. At 72 h after treatment, cell viability was assessed using CCK-8 assay (Dojindo Laboratories, Kumamoto, Japan) in accordance with the manufacturer's instructions. Absorbance was detected at 450 nm using the VersaMax microplate reader (Molecular Devices, Sunnyvale, CA, USA).

4. Cell Cycle Analysis

Cells were treated with mJX-594 for 24 h. To analyze the cell cycle, treated cells were harvested, washed in phosphate-buffered saline (PBS), resuspended in ice-cold 70% ethanol, and then incubated overnight. Ethanol was removed, and cells were washed with PBS prior to staining with PI/RNase staining buffer (BD Pharmingen, Franklin Lakes, NJ, USA). Cells were incubated for 15 min at room temperature and analyzed on a BD LSR II cell analyzer (BD Biosciences, San Jose, CA, USA). Cell cycle modeling was performed

연세대학교
YONSEI UNIVERSITY

using FlowJo v10 software (FlowJo LLC, Ashland, OR, USA).

5. TUNEL, Migration, and Invasion Assay

For apoptotic cell analysis, PBS- or mJX-594-treated cells were washed with PBS, fixed in 4% paraformaldehyde for 15 min at room temperature, and permeabilized with 0.3% Triton X-100 for 5 min. Apoptotic cells with DNA breaks were detected using the In Situ Cell Death Detection Kit, TMR red (#12 156 792 910; Roche, Indianapolis, IN, USA) according to the supplier's protocol. For migration assay, cells were treated with PBS or mJX-594 (1 MOI) and plated in the top chamber (5×10^4 cells/well) of 24-well Transwell (8.0 μm pore size; Corning Inc., Corning, NY, USA). Then, a 10% fetal bovine serum-containing medium was placed in the bottom Transwell chamber, and the assembly was incubated at 37 ℃ for 24 h. In vitro Matrigel invasion assays were performed using CytoSelect™ 24-Well Cell Invasion Assay kit (Cell Biolabs, San Diego, CA, USA) following the manufacturer's manual. Migrating or invading cells on the bottom surface of the membrane were stained with crystal violet and quantified at OD 560 nm after extraction using the VersaMax microplate reader (Molecular Devices, Sunnyvale, CA, USA).

6. Development of Orthotopic Tumor Models and Treatments

The protocol was approved by the Institutional Animal Care and Use Committee (IACUC) of the Yonsei University Health System (IACUC No. 2020-0006) which follows the guidelines specified by the Institute of Laboratory Animal Resources Commission on Life Sciences National Research Council in the USA. All animal experiments were conducted following the Guide for the Care and Use of Laboratory Animals.

Adult male BALB/c mice (Orient Bio Inc., Seongnam, GyeongGi-Do, Korea) aged 6–7 weeks were used in this study. We used highly pulmonary orthotopic RCC murine models that were previously developed by our team.[29] To develop a clinically relevant murine RCC model that exhibited enhanced pulmonary metastasis, mice underwent intrarenal implantation using Renca cells (1×10^5 cells/100 μL), and an in vivo selection of tumor cells from pulmonary metastases for reimplantation was performed, which is described

연세대학교
YONSEI UNIVERSITY

elsewhere in detail.[29] Using this model, two models were developed (Figure 1). The first was the early-stage mRCC model, which started receiving the treatment either by mJX-594 (group A) or sunitinib (group B) after the 1st day of implantation of in vivo selected tumor cells. The second was the advanced-stage mRCC model, which started receiving the treatment either by mJX-594 (group C) or sunitinib (group D) after the 11th day of implantation of in vivo selected tumor cells. mJX-594 (1×10^7 plaque-forming units [pfu] per mouse) was intraperitoneally injected every 3 days for three times. The mice in the control group were treated with the same volume of mJX-594 for PBS every 3 days for three times. For the experiments of angiogenesis inhibitors, the mice received sunitinib (40 mg/kg in 5 μL/g sterile saline with 0.5% methylcellulose suspension per mouse) by gavage daily for 7 days. After the 21st day (3 weeks) of injection, the mice were sacrificed, and their kidney tissues were harvested and weighed. Their lungs were inflated with India ink to visualize lung tumor nodules.

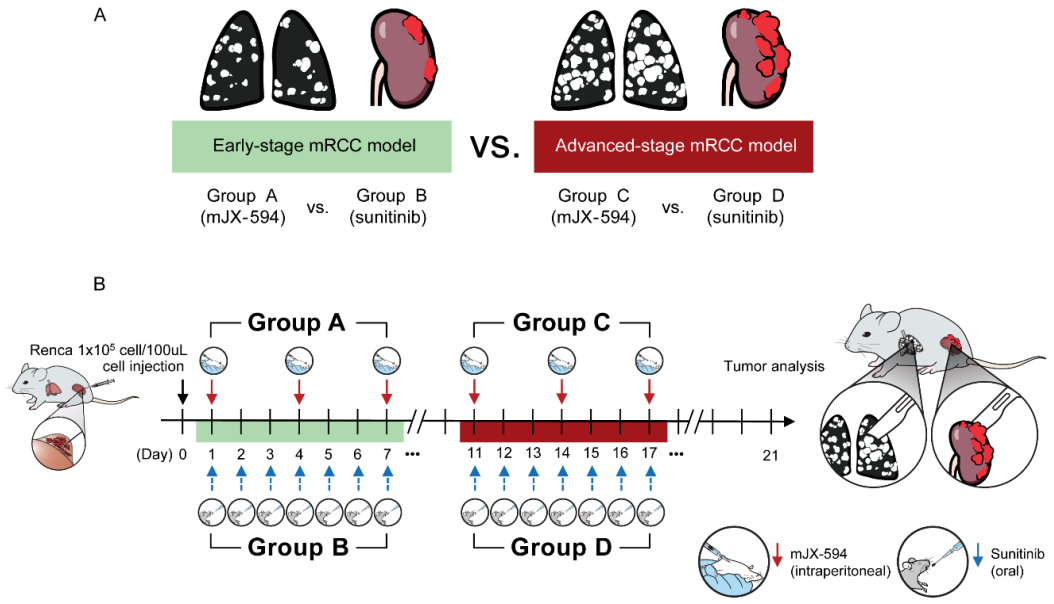

Figure 1. Two pulmonary metastatic orthotopic renal cell carcinoma murine models. (A) An early-stage metastatic renal cell carcinoma (mRCC) model was used to compare groups A (mJX-594 monotherapy) and B (sunitinib monotherapy). The advanced-stage mRCC

연세대학교
YONSEI UNIVERSITY

model was used to compare groups C (mJX-594 monotherapy) and D (sunitinib monotherapy). (B) In vivo selected tumor cells from pulmonary metastases for reimplanted (1×10^5 cells/100 μL) and treatments started on the first day of implantation for groups A and B. For groups C and D, treatments started on the 11th day of implantation. mJX-594 was intraperitoneally injected every 3 days for three times, whereas sunitinib was treated by gavage daily for 7 days. After the 21st day of injection, analysis was performed.

7. IFN-ɣ Enzyme-Linked Immunospot (ELISPOT) Assay

For measurement of tumor-specific cytotoxic T cells, splenocytes and tumor-infiltrating lymphocytes (TILs) from each group were isolated 3 days after the final treatments. Cells were labeled with anti-CD8a microbeads (Miltenyi Biotec, Auburn, CA, USA), then purified using MACS (Miltenyi Biotec). CD8+ T cells were enriched to more than 90% purity and purified CD8+ T cells were co-cultured with Renca tumor cells (10:1 ratio) in 96-well plates which are precoated with mouse IFN-ɣ (Mabtech, Inc., Cincinnati, OH, USA). Plates were incubated with 1 μg/mL of the biotinylated anti-mouse IFN-ɣ antibody R4-6A2-biotin for 2 h at room temperature then addition and incubation of streptavidin-ALP solution for 1 h at room temperature. Finally, spots were analyzed using ImageJ software after the addition of BCIP/NBT-plus substrate solution.

8. Immunofluorescence Staining

Immunofluorescence staining was performed in the advanced-stage mRCC model since significant therapeutic efficacy of JX-594 monotherapy was observed in the advanced-stage model. Tissues were fixed in 10% formalin overnight and then transferred to 70% ethanol. The samples were paraffin-embedded, sectioned, and stained using the following primary antibodies: rabbit anti-CD31 (EPR17260-263; Abcam, Cambridge, MA, USA), rat anti-CD8 (YTS169.4; Abcam), rat anti-CD4 (RM4-5; BD Pharmingen), rabbit anti-PD-L1 (EPR20529; Abcam), mouse anti-cytokeratin (C11; Santa Cruz Biotechnology, Santa Cruz, CA, USA), rat anti-Foxp3 (FJK-16s; Invitrogen, Waltham, MA, USA), hamster anti-CD11c (HL3; BD Pharmingen), and rabbit anti-VV (Abcam). After washing, the slides

연세대학교
YONSEI UNIVERSITY

were incubated with the following secondary antibodies: FITC-conjugated or Texas Red-conjugated anti-rabbit IgG (Vector Laboratories, Burlingame, CA, USA), FITC-conjugated anti-rat IgG (Jackson ImmunoResearch, West Grove, PA, USA), Texas Red-conjugated anti-mouse IgG (Vector Laboratories), or FITC-conjugated anti-hamster IgG (Jackson ImmunoResearch). Finally, the samples were mounted with VECTASHIELD® Mounting Medium (Vector Laboratories). The immunofluorescence images were captured using the Zeiss LSM700 confocal microscope (Carl Zeiss Microscopy GmbH, Jena, Germany). Staining was quantified using the ImageJ software. Signal intensity was calculated as the number of positive-staining pixels relative to the total number of pixels per tumor section (% positive).

9. Development of Cell-Line Derived Xenograft (CDX) Tumor Models and Treatments

As shown in Figure 2, a total of 64 adult male BALB/c nude mice (Orient Bio Inc., Seongnam, GyeongGi-Do, Korea) aged 6−7 weeks were maintained in clean animal facilities at Yonsei University Health System. Tumors were implanted by subcutaneous injection of 0.2−1.0 x 10^7 cells into the right flank of the mice. Among 64 mice, 32 mice were treated with JX-594 (test group) and another 32 mice were treated with phosphate-buffered saline (PBS) as the control group. For both the test and control group, 8 mice were allocated for each group according to the most commonly mutated genes (*VHL, PBRM1, SETD2,* and *BAP1*). After the 18th day of injection, the mice were sacrificed, and their tumor tissues were harvested.

When tumors reached > 50 mm^3, mice were treated with either PBS or 1 x 10^7 plaque-forming units of JX-594 by intratumoral injection in day 0, 3, and 6. Tumors were measured by digital caliper every 3 days and tumor volumes were calculated using the modified ellipsoid formula [1/2 x (length x $width^2$)]. Tumor growth rate was calculated by the increased tumor volume divided by the day which was measured between day 0 and 12. The decreased tumor volume by JX-594 was measured by the decreased tumor volume during the day 3 through 12. Relative therapeutic response ratio was calculated by the formula (decreased tumor volume x tumor growth rate) in order to adjust the relative

연세대학교
YONSEI UNIVERSITY

differences in tumor growth rate of each cell line and compare the actual therapeutic effects of JX-594 in each cell line.

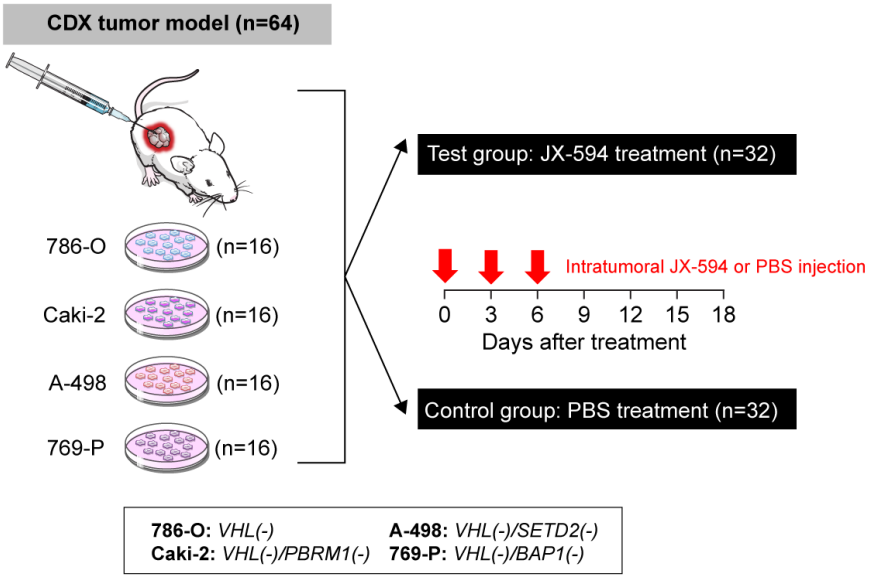

Figure 2. Development of cell-line derived xenograft tumor models according to four most commonly mutated genes (*VHL*, *PBRM1*, *SETD2*, and *BAP1*) in clear cell renal cell carcinomas. Mice were subcutaneously injected with tumor cells in the right flank and JX-594 was intratumorally injected on day 0, 3, and 6 after the tumor cell injection for the test group and PBS was intratumorally injected for the control group.

10. Interferon beta (IFN-β) expression in four most commonly mutated genes in ccRCC cell lines

mRNA expression levels of interferon beta (IFN-β) were measured by qRT-PCR in four most commonly mutated ccRCC cell lines (786-O, Caki-2, A-498 and 769-P) after JX-594 and control (PBS) treatments. Total RNA was extracted from cells using TRIzol® reagent (Ambion, Life Technologies, USA). 1 μg of RNA sample was reverse-transcribed into first-strand cDNA using an iNtRon Maxime RT PreMix (Intronbio. Cat No. 25082) according

연세대학교
YONSEI UNIVERSITY

to the manufacturer's protocol. qRT-PCR was performed using the Power SYBR® Green Master Mix (Thermo Fisher, Cat No. A25742, USA) in a 10-μL reaction volume comprising 5 μL of SYBR® Green master PCR mix, 1 μL of each forward and reverse primer (10 pmol), 1 μL of diluted cDNA template, and sterile distilled water. The PCR primer sequences are presented in Table 1. Conditions for amplification were as follows: initial denaturation at 95 ℃ for 10 min; 40 cycles of denaturation at 95 ℃ for 15 s, annealing at 58 ℃ for 60 s, and elongation at 72 ℃ for 60 s; final elongation at 72 ℃ for 5 min. qRT-PCR was performed on the ABI StepOnePlus Real-Time PCR System (Applied Biosystems, Foster City, CA, USA). All quantifications were performed with GAPDH as a reference gene for standardization of relative expression levels. Relative gene expression was analyzed using the $2^{-\Delta\Delta C}{}_{T}$ method, and the results are expressed as the percent change with respect to control values. At least three replicates of qRT-PCR experiments were performed, and the results were analyzed by a blinded investigator.

11. Statistical Analysis

Statistical analyses were performed using GraphPad Prism version 8.0 (GraphPad Software, Inc., La Jolla, CA, USA) and SPSS version 23.0 (IBM Corp., Armonk, NY, USA). All results were expressed as the mean ± standard deviation (s.d.) unless otherwise indicated. Student’s t-test was used unless the dataset did not follow a normal distribution on a Shapiro-Wilk normality test. If the dataset did not follow a normal distribution, the Mann-Whitney U test was used. All statistical tests were two-tailed, and p-values < 0.05 were considered significant.

연세대학교
YONSEI UNIVERSITY

III. RESULTS

1. Effect of JX-594 in Human and Murine RCC Cell Lines Resulting in Cytotoxicity, Cell Cycle Arrest, and Decrease in Migration and Invasion Ability

Treatment of 786-O, Caki-1, A-498, and ACHN with JX-594 resulted in a dose-dependent decrease in cell viability at 72 h post-treatment (Figure 3A). Similar to the human RCC cell lines, infection of Renca cells with mJX-594 resulted in cytotoxicity (Figure 3A). Following treatment of mJX-594, Renca cells resulted in a significant increase in G2/M-phase cells (38.6 ± 8.5% vs. 27.9 ± 3.0%, $p < 0.05$), known as G2/M-phase arrest (Figure 3B). Terminal deoxynucleotidyl transferase-mediated dUTP nick-end labeling (TUNEL) assay revealed significantly increased apoptosis ($p < 0.01$; Figure 3C). The migration ability of Renca cells decreased after treatment with mJX-594, with a significantly lower repair with the starch test compared with that in the control group ($p < 0.01$; Figure 3D). The number of invasive Renca cells penetrating the membrane after treatment for 24 h with mJX-594 was significantly lower compared with that in the control group ($p < 0.01$; Figure 3E).

연세대학교
YONSEI UNIVERSITY

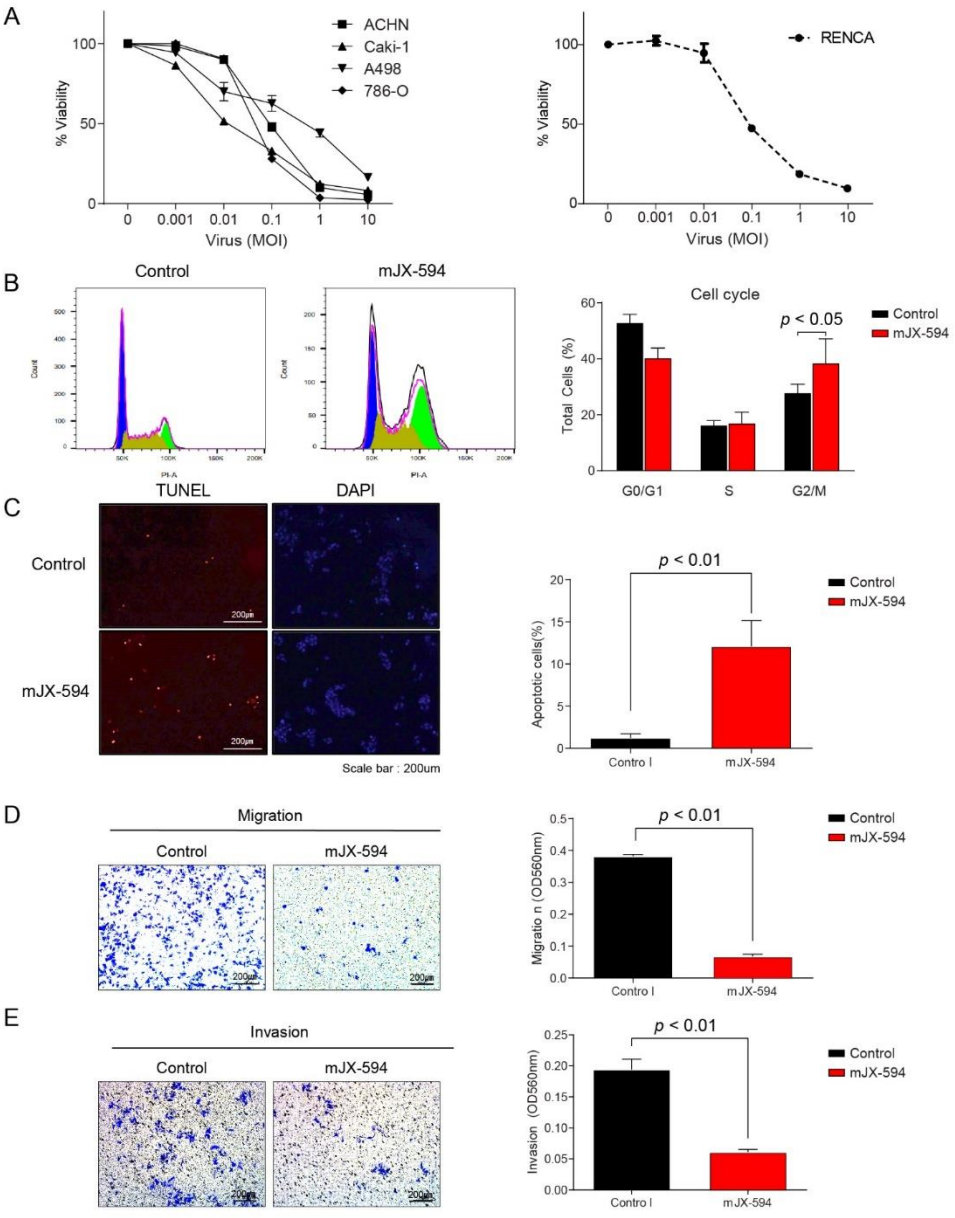

Figure 3. JX-594 has a direct oncolytic effect against human and murine renal cell carcinoma (RCC). (A) Cell viability of human (786-O, A498, ACHN, Caki-1) and murine (Renca) RCC cell lines treated with escalating doses of JX-594 or mJX-594. (B) Cell cycle

연세대학교
YONSEI UNIVERSITY

analyses of mJX-594-treated cells. Renca cells treated with mJX-594 (1 MOI) were analyzed by flow cytometry for DNA content at 24 h post-treatment. Representative cell cycle histograms (left) and quantification of cell cycle distribution (right). (C) Apoptosis of Renca cells treated with mJX-594 or control (PBS) was analyzed using the TUNEL assay; TUNEL-positive cells (pseudocolored red), nuclei (pseudocolored blue), scale bar: 200 μm. (D) Migration of Renca cells was evaluated and compared after the treatment with mJX-594 or control (PBS), scale bar: 200 μm. (E) Invasion of Renca cells was evaluated and compared after the treatment with mJX-594 or control (PBS), scale bar: 200 μm. Values are mean ± SD. PBS, phosphate-buffered saline. All experiments were conducted at least three times.

2. Comparison of Therapeutic Efficacy of JX-594 and Sunitinib in Early- and Advanced-Stage mRCC

To demonstrate and compare the therapeutic efficacy of mJX-594 or sunitinib monotherapy between the favorable-risk group and the intermediate- or poor-risk group according to the IMDC criteria, we developed two models (Figure 1 and Table 1). The early-stage model was designed to resemble the favorable-risk group, and the advanced-stage model reflected the intermediate or poor-risk group (Figure 1). mJX-594 and sunitinib treatments reduced the primary tumor burden (Figure 4A) and metastatic lung lesions (Figure 4B) in early-stage mRCC. In advanced-stage mRCC, mJX-594 treatment reduced the primary tumor burden (Figure 4C) and metastatic lung lesions (Figure 4D), but no therapeutic effects were observed with sunitinib monotherapy.

연세대학교
YONSEI UNIVERSITY

Table 1. Comparison of therapeutic efficacy of JX-594 and sunitinib monotherapy in early- and advanced-stage metastatic renal cell carcinoma models.

	Early-Stage		**Advanced-Stage**	
IMDC Criteria	**Favorable-Risk Group**		**Intermediate- or Poor-Risk Group**	
	Primary tumor	Metastatic sites	Primary tumor	Metastatic sites
JX-594	(+)	(+)	(+)	(+)
Sunitinib	(+)	(+)	(-)	(-)

(+) denotes superior therapeutic efficacy compared with the control group. (-) denotes no superior therapeutic efficacy compared with the control group.

In early-stage mRCC, mJX-594 treatment significantly reduced both the primary tumor burden ($p < 0.01$) and metastatic lung lesions ($p < 0.05$) than did the control (Figure 4E, F). Similarly, sunitinib treatment significantly reduced the primary tumor burden ($p < 0.05$) and metastatic lung lesions ($p < 0.05$) than did the control (Figure 4E, F). Regarding the therapeutic efficacy for primary tumor lesions, no statistical differences were observed between the mJX-594 and sunitinib treatments (Figure 4E). In terms of the therapeutic efficacy for metastatic lung lesions, mJX-594 treatment demonstrated significantly better outcomes than those of sunitinib treatment ($p < 0.05$) (Figure 4F).

In advanced-stage mRCC, mJX-594 treatment significantly reduced the primary tumor burden ($p < 0.01$) and metastatic lung lesions ($p < 0.01$) than did the control (Figure 4G, H). Sunitinib treatment also reduced the primary tumor burden and metastatic lung lesions than did the control, but no statistical differences were found. mJX-594 treatment demonstrated superior efficacy compared with sunitinib treatment in terms of the primary tumor burden and metastatic lung lesion reduction in advanced-stage mRCC.

To determine whether systemic injection of JX-594 could induce both primary tumor and distant lung metastatic site immune responses, we administered mJX-594 into the peritoneum. Systemic injection of mJX-594 was generally well-tolerated without significant weight loss, and no treatment-related mortalities were observed (Figure 5).

연세대학교
YONSEI UNIVERSITY

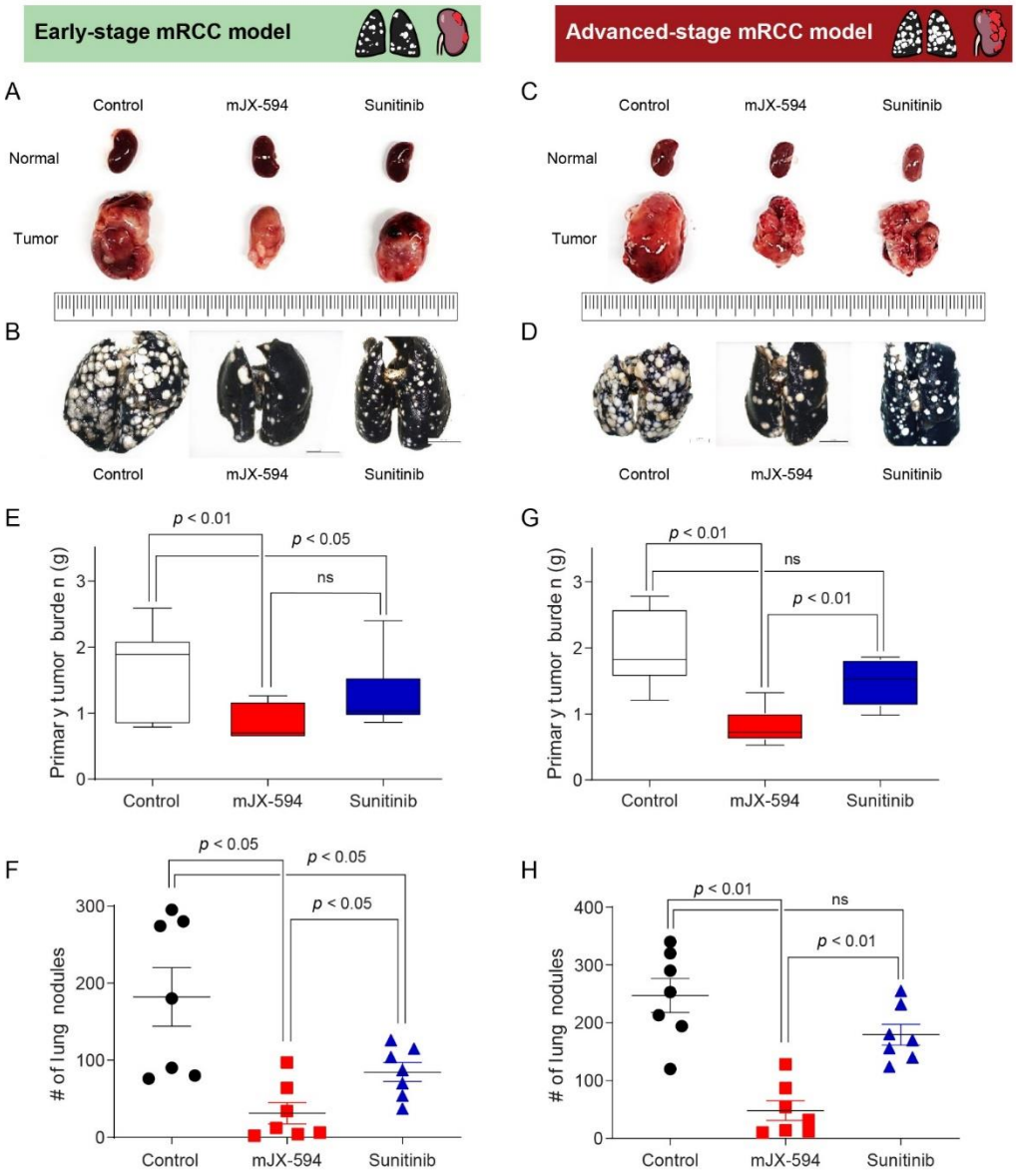

Figure 4. Representative images and comparisons of primary tumor burden and number of lung nodules in mJX-594-treated, sunitinib-treated, and control (PBS-treated) mice. (A) Comparison of primary tumor burden after the treatments in early-stage metastatic renal cell carcinoma (mRCC) model. (B) Comparison of lung metastasis after the treatments in early-stage mRCC model. (C) Comparison of primary tumor burden after the treatments in

연세대학교
YONSEI UNIVERSITY

advanced-stage mRCC model. (D) Comparison of lung metastasis after the treatments in advanced-stage mRCC model. Therapeutic efficacy of mJX-594 and sunitinib treatment in early- and advanced-stage mRCC models. (E) Comparison of primary tumor burden after the treatments with mJX-594, sunitinib, or control (PBS) in early-stage mRCC model. (F) Comparison of lung metastasis after the treatments with mJX-594, sunitinib, or control (PBS) in early-stage mRCC model. (G) Comparison of primary tumor burden after the treatments with mJX-594, sunitinib, or control (PBS) in advanced-stage mRCC model. (H) Comparison of lung metastasis after the treatments with mJX-594, sunitinib, or control (PBS) in advanced-stage mRCC model. Values are mean ± SD. PBS, phosphate-buffered saline; ns, not significant; #, number.

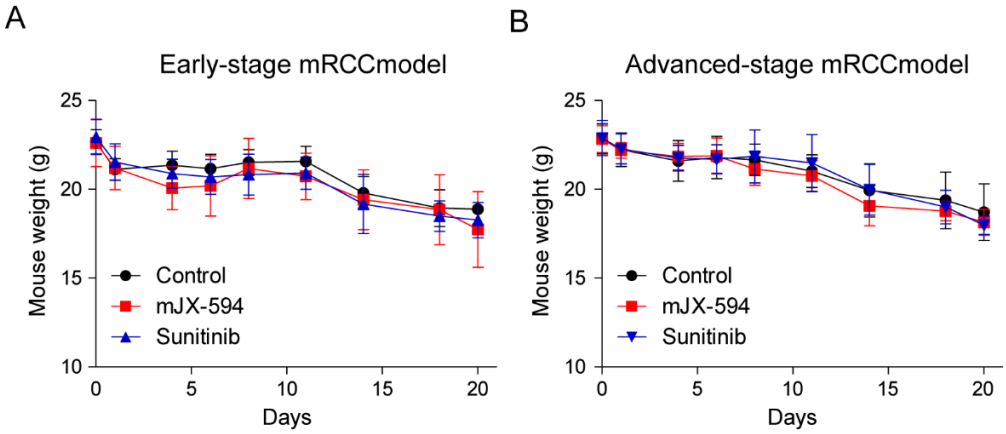

Figure 5. Mice weight over time, demonstrating no significant weight loss in JX-594 or sunitinib treatment group compared with control group according to (A) early-stage metastatic renal cell carcinoma (mRCC) model and (B) advanced-stage mRCC model.

3. JX-594 Systemic Treatment Increases Local Cancer-Specific Immune Responses by Converting Immunosuppressive Noninflamed Tumors into Inflamed Tumors in Primary Tumor

연세대학교
YONSEI UNIVERSITY

To determine the immunomodulatory potential of JX-594 in the therapeutic efficacy of primary tumor, changes in the TME of the primary tumor after systemic treatment of mJX-594 were evaluated (Figure 6). The tumoral level of mJX-594 was significantly increased, whereas tumor vessel density was significantly reduced after the mJX-594 treatment. The population of CD8+ cytotoxic T cells within the tumor, which comprise the most critical aspect of anticancer immunity, increased after the mJX-594 treatment. CD4+ T cells and CD11c+ dendritic cells (DCs) also increased after the mJX-594 treatment. The number of Foxp3+ regulatory T cells (Treg) reduced after the mJX-594 treatment. Conversely, the inhibitory checkpoint molecule, PD-L1, significantly increased. Collectively, noninflamed tumors were converted into T cell-inflamed tumors by JX-594 systemic treatment.

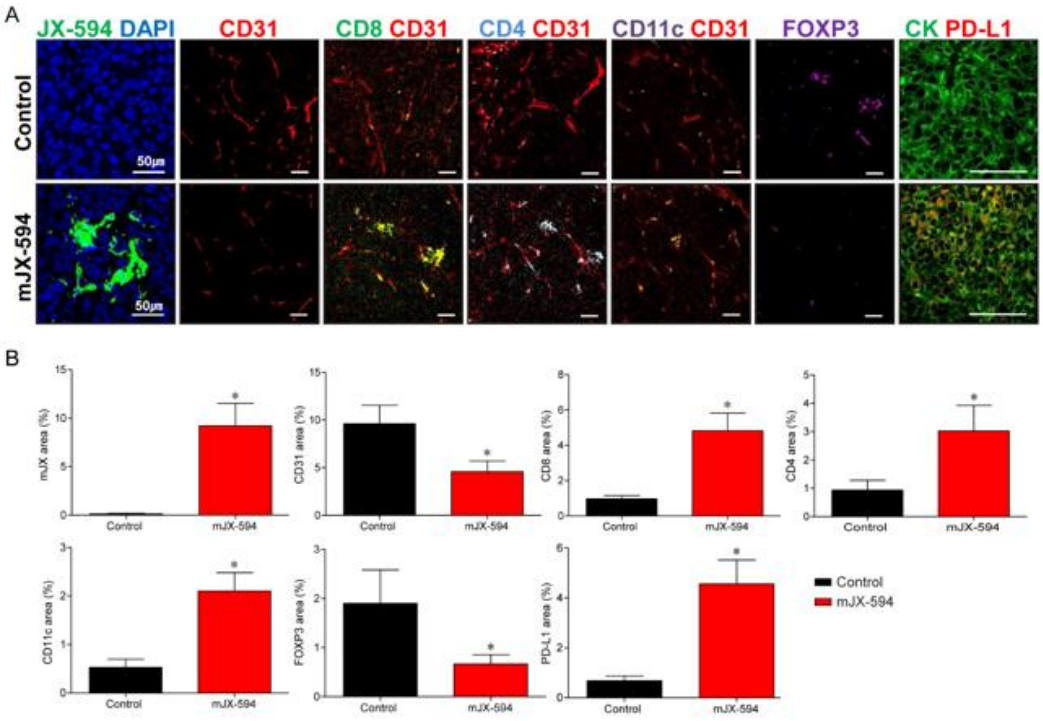

Figure 6. mJX-594 systemic treatment activates anti-cancer immunity by converting immunosuppressive noninflamed tumors into inflamed tumors at primary tumor. (A) Representative images of primary tumors treated with mJX-594 systemic treatment. Tumor sections were stained for JX-594, CD31, CD8, CD4, CD11c, Foxp3, and PD-L1. Scale bars,

연세대학교
YONSEI UNIVERSITY

50 μm. (B) Quantifications of the JX-594+ area, CD31+ blood vessels, CD8+ T cells, CD4+ T cells, CD11c+ dendritic cells, Foxp3+ regulatory T cells, and PD-L1+ cells. Values are mean ± SD. * $p < 0.05$ vs. control. 6 animals per group were used.

4. Systemic Injection of JX-594 Leads to Distant Lung Metastatic Sites Cancer-Specific Immune Responses

Immunofluorescence analyses revealed similar alterations in the innate and adaptive immunity in the lung metastatic sites (Figures 7 and 8 (high-magnification version)), which was demonstrated in the primary tumor. Regarding innate immunity, mJX-594 treatment significantly increased the number of DCs 4.2-fold ($p < 0.001$). Similarly, mJX-594 treatment increased the adaptive immunity by increasing the number of CD8+ cytotoxic T cells 4.8-fold and that of CD4+ T cells 3.3-fold compared with those of the control group, with statistical significance ($p < 0.001$). Collectively, these findings indicate that JX-594 treatment effectively suppressed the progression of lung metastatic lesions via enhanced innate and adaptive immunity.

연세대학교
YONSEI UNIVERSITY

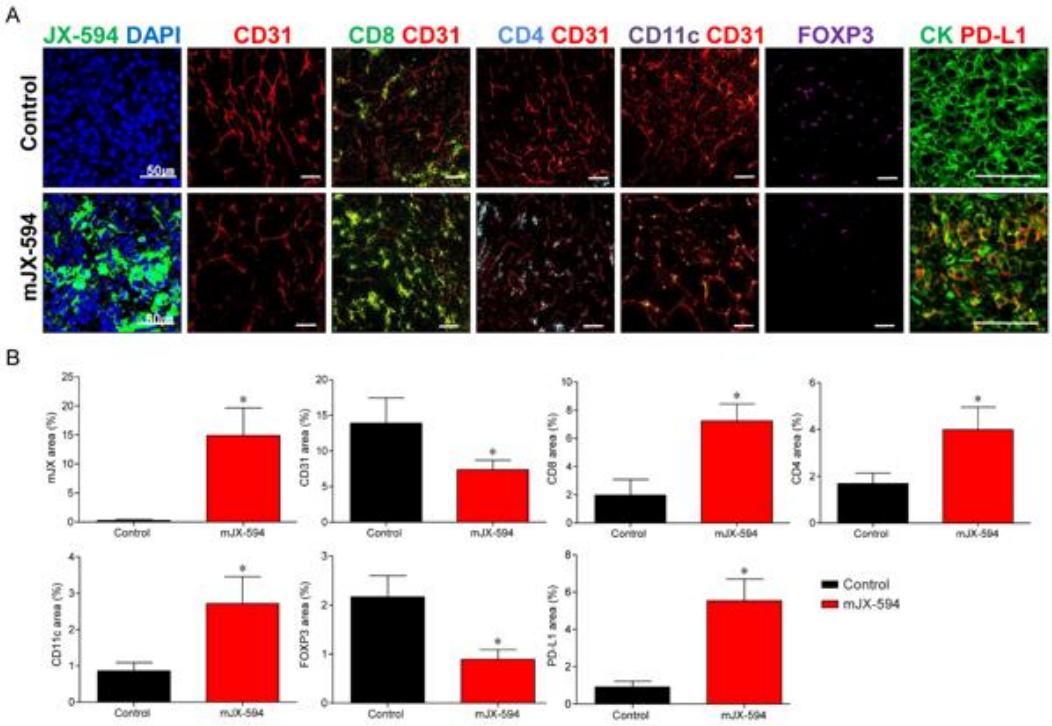

Figure 7. mJX-594 systemic treatment activates anti-cancer immunity by converting immunosuppressive noninflamed tumors into inflamed tumors at lung metastatic sites. (A) Representative images of lung metastatic sites treated with mJX-594 systemic treatment. Tumor sections were stained for JX-594, CD31, CD8, CD4, CD11c, Foxp3, and PD-L1. Scale bars, 50 μm. (B) Quantifications of the JX-594+ area, CD31+ blood vessels, CD8+ T cells, CD4+ T cells, CD11c+ dendritic cells, Foxp3+ regulatory T cells, and PD-L1+ cells. Values are mean ± SD. * $p < 0.05$ vs. control. 6 animals per group were used.

연세대학교
YONSEI UNIVERSITY

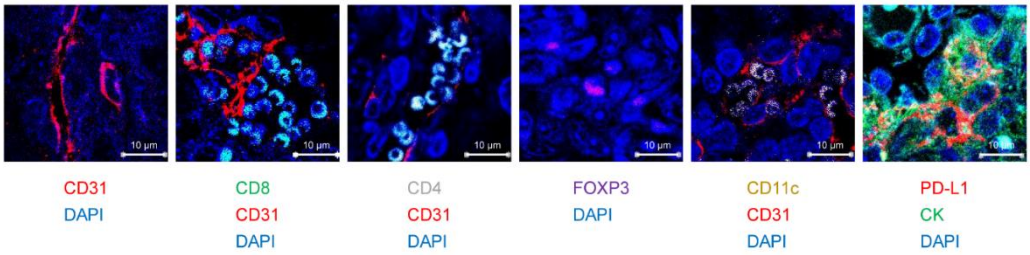

Figure 8. Representative high-magnified images of lung metastatic sites treated with mJX-594 systemic treatment. Tumor sections were stained for CD31, CD8, CD4, CD11c, Foxp3, and PD-L1. Scale bars, 10 μm.

5. Comparison of Changes in TME between Primary Tumor and Lung Metastatic Sites

Changes in the TME between the primary tumor and lung metastatic sites were compared (Table 2). mJX-594 increased 49.7- and 92.0-fold in the primary tumor and lung metastatic sites, respectively, demonstrating more significant increases in the tumor level of JX-594 in lung metastatic sites ($p = 0.028$). Increases in terms of fold changes in CD4/CD8+ T cells and CD11c+ DCs in the lung metastatic sites were significantly higher than those in the primary tumor (CD8+ T cells: $p = 0.019$, CD4+ T cells: $p = 0.004$, CD11c+ DCs: $p = 0.017$). No significant differences were noted in terms of fold changes in the CD31+ blood vessel, Foxp3+ Treg, and PD-L1+ cells between the primary tumors and lung metastatic sites.

IFN-ɣ ELISPOT assays have shown a significant increase in IFNγ-secreting T cells against Renca tumor cells within primary tumors, lung metastatic sites, and spleens of JX-594 treated mice compared with control mice (Figure 9).

연세대학교
YONSEI UNIVERSITY

Table 2. Comparison of changes in the TME between the primary tumor and lung metastatic sites

	Fold-Change (JX-594/Control)		***p*-Value**
Primary tumor	mJX-594	49.7	< 0.001
	CD31+ blood vessel	0.5	0.002
	CD8+ T cells	3.6	< 0.001
	CD4+ T cells	2.4	< 0.001
	CD11c+ DCs	3.0	< 0.001
	Foxp3+ Treg	0.4	< 0.001
	PD-L1+ cells	6.1	< 0.001
Lung metastatic sites	mJX-594	92.0	< 0.001
	CD31+ blood vessel	0.5	< 0.001
	CD8+ T cells	4.8	< 0.001
	CD4+ T cells	3.3	< 0.001
	CD11c+ DCs	4.2	< 0.001
	Foxp3+ Treg	0.4	0.002
	PD-L1+ cells	6.6	< 0.001

p-value was calculated between JX-594 vs. control.

연세대학교
YONSEI UNIVERSITY

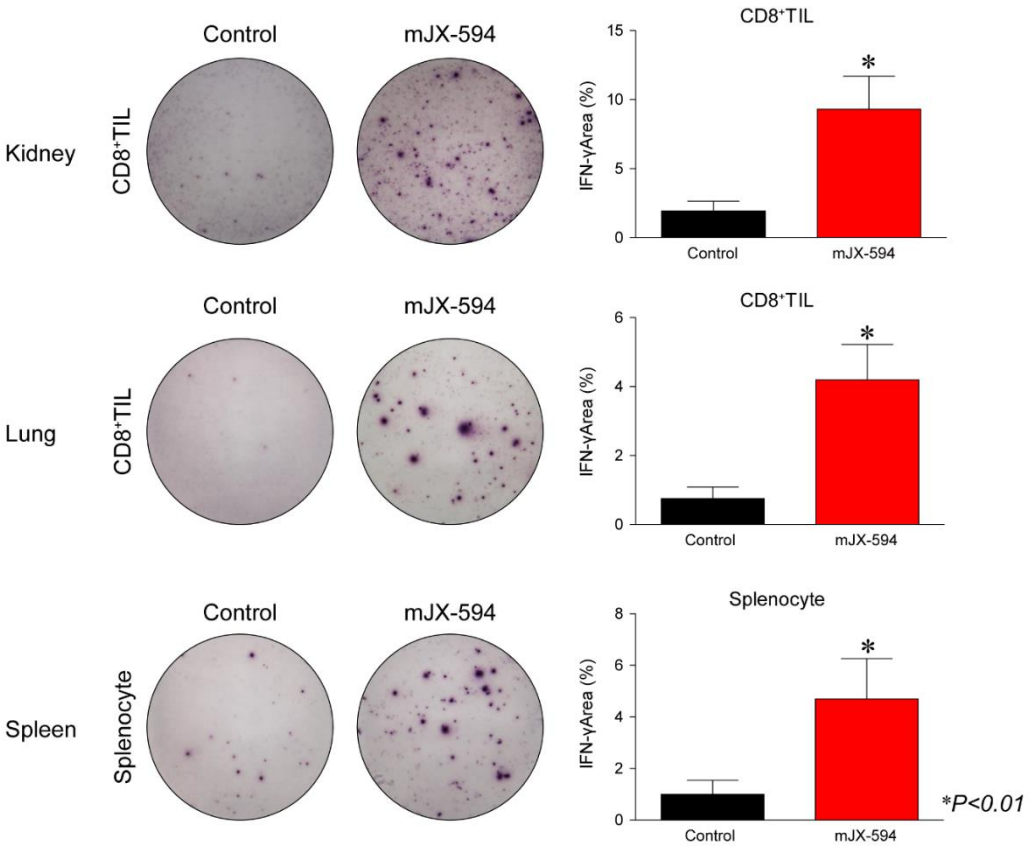

Figure 9. Images and comparisons of IFNγ ELISPOT in CD8+ tumor infiltrating lymphocytes (TILs) and splenocytes from control or JX-594 treated mice. CD8+ TILs were isolated from dissociated tumors with anti-CD8 antibody-coated magnetic beads. * P < 0.01.

연세대학교
YONSEI UNIVERSITY

6. Comparison of therapeutic efficacy of JX-594 according to genetic mutations in CDX models

All four CDX models demonstrated significant decrease in tumor size by the JX-594 treatment compared to PBS treatment from day 9 after the JX-594 treatment (Figure 10A).

For subgroup analysis by genetic mutations, CDX model with *BAP1* mutation reported the most rapid tumor growth rate compared to *VHL, PBRM1,* and *SETD2* mutation with statistical significance ($P < 0.01$; Figure 10B). CDX model with *PBRM1* mutation demonstrated the slowest tumor growth rate compared to other genetic mutations with statistical significance ($P < 0.01$; Figure 10B).

The decrease in tumor volume by JX-594 treatment was most significant in *BAP1* mutation tumor compared to other tumors with mutations in *VHL, PBRM1,* and *SETD2* ($P < 0.01$; Figure 10C). Otherwise, *SETD2* mutation tumor demonstrated the least decrease in tumor volume by JX-594 compared to other mutations ($P < 0.01$; Figure 10C).

In terms of relative therapeutic response ratio (Figure 10D), which adjusted the relative difference in a tumor growth rate of each cell line, *BAP1* mutation was associated with significantly better relative therapeutic response ratio compared to tumors with other mutations. Furthermore, no statistical difference in relative therapeutic response ratio was observed between *PBRM1* and *SETD2* mutation tumor.

연세대학교
YONSEI UNIVERSITY

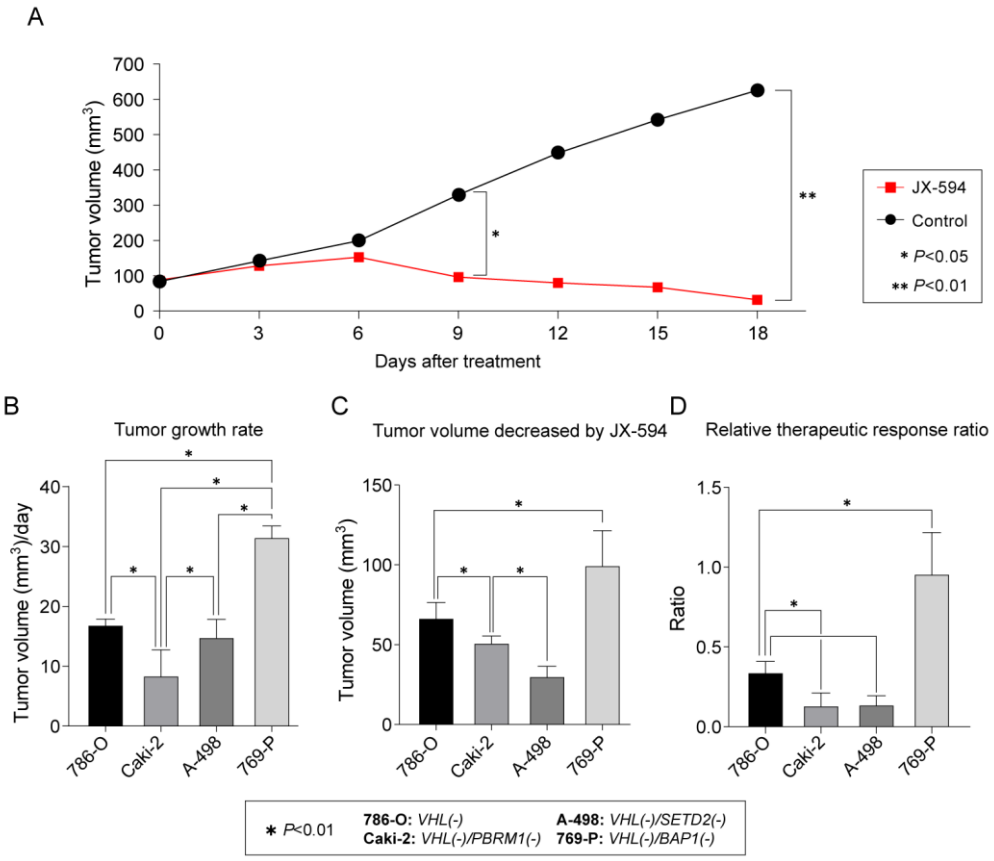

Figure 10. Evaluation of cell-line derived xenograft tumor models treated with JX-594 or control (PBS) treatment. (A) Growth curves of JX-594 and control treatment groups. Bar graphs representing (B) tumor growth rate in control treatment group, (C) decrease in tumor volume by JX-594 treatment group, and (D) relative therapeutic response ratio (decreased tumor volume x tumor growth rate) to JX-594 treatment according to *VHL*, *PBRM1*, *SETD2*, and *BAP1* mutations.

7. Comparison of IFN-β expression levels after the JX-594 treatment according to genetic mutations in ccRCC cell lines

mRNA expression levels of IFN-β were measured after the JX-594 or control (PBS) treatment in four most commonly mutated ccRCC cell lines. IFN-β expression level was

연세대학교
YONSEI UNIVERSITY

significantly decreased in *BAP1*-deficient cell line compared to other cell lines in the control treatment group (Figure 11A). The IFN-β expression levels were overall increased after JX-594 treatment in all cell lines, and *BAP1*-deficient cell line has the highest recovery rate (Figure 11B).

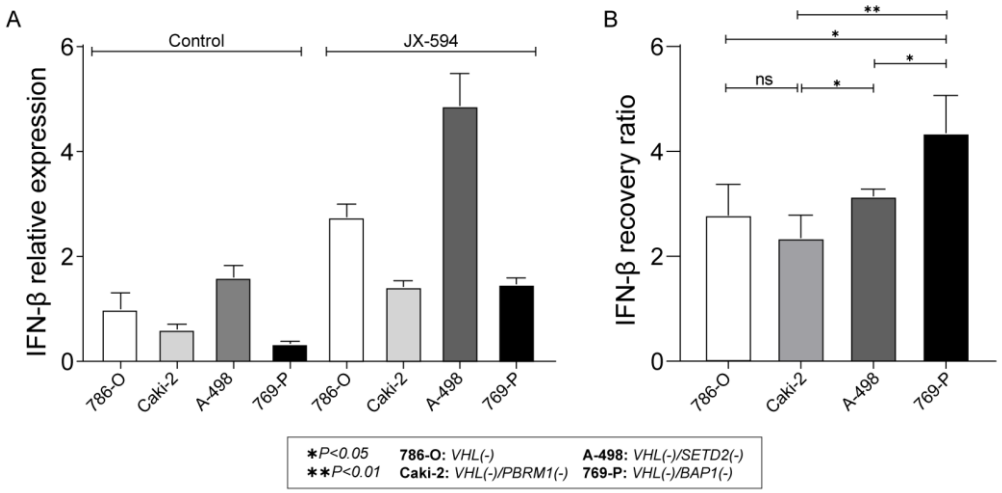

Figure 11. IFN-β mRNA expression levels of four most commonly mutated genes in ccRCC cell lines. (A) Measurement of IFN-β expression levels in after JX-594 or control (PBS) treatment. (B) IFN-β recovery ratio of ccRCC cell lines calculated as IFN-β levels after JX-594 treatment dived by control (PBS) treatment.

IV. DISCUSSION

In this study, we demonstrated that the systemic delivery of JX-594 monotherapy was an effective therapeutic strategy for mRCC, both reducing the primary tumor burden and lung metastatic sites without adverse reactions. Although the combination therapy with ICI was not within the scope of this study and was therefore not evaluated here, JX-594 monotherapy itself sufficiently converted noninflamed tumors to inflamed tumors, enabling the host immune system to eradicate the tumor cells. Our findings provide evidence that the oncolytic vaccinia virus, JX-594, is an effective therapeutic modality not only in early-stage mRCC but also in advanced-stage mRCC by changing the TME to

연세대학교
YONSEI UNIVERSITY

stimulate host immune responses against the tumor. Sunitinib, which remains the first-line therapy for mRCC, has also exhibited therapeutic efficacy in early-stage mRCC both in the primary tumors and lung metastatic sites. Furthermore, *BAP1* mutation tumor demonstrated the biggest therapeutic benefits from JX-594, suggesting *BAP1* as the potential for predictive biomarkers for JX-594 treatments.

Viruses have evolved to evade the host immune responses after years of co-evolution with our immune systems.[30] With their evolution and the advancement of technology, viruses, namely OVs, have been therapeutically engineered to fight against cancers.[12] OVs selectively infect and kill the cancer cells without disrupting the normal cells.[17,31] They induce direct destruction of tumors through selective infection and tumor-cell lysis.[6,32] During this process, immunogenic cell death occurs with the widespread release of tumor-associated antigens.[6] These antigens are presented by the DCs to activate the antitumor immunity by inducing antigen-specific T-cell responses with the expansion of cytotoxic effector cells, eventually acting as an in situ cancer vaccine within the TME.[33]

In our study, JX-594 effectively remodeled the TME both in the primary tumors (Figure 6) and distant lung metastatic sites (Figure 7) through the activation of the immune system, which increased the tumor-infiltrating CD4/8+ T cells and DCs. JX-594 is known for its tumor control ability by T cell-mediated mechanism rather than direct oncolysis.[17] Our study also demonstrated that the activation of antitumor immunity significantly induced the regression of the primary tumor burden and the number of lung metastases through T cell-mediated mechanism, demonstrating the therapeutical benefits of JX-594 systemic injection.

Few OVs have been evaluated in many preclinical and clinical studies, and talimogene laherparepvec (Imlygic) was the first oncolytic herpesvirus to be approved and clinically used for the treatment of advanced melanoma.[34] For JX-594, a phase Ib clinical trial (NCT03294083) addressed patients with mRCC treated with IV infusion of JX-594 combined with cemiplimab (anti-PD-1), which reported an overall response rate of 37.5% with an acceptable safety profile in an American Association for Cancer Research meeting.[35]

JX-594 activated the anticancer immunity; however, the inhibitor checkpoint molecule, PD-L1, was increased, suggesting the induction of negative feedback mechanisms to

연세대학교
YONSEI UNIVERSITY

counter-balance the immune response in the TME. A similar result was reported by Chon et al. wherein PD-L1 upregulation immediately followed a massive influx of CD8+ T cells.[17] Therefore, the combinatorial use of ICIs seems plausible considering the upregulated inhibitor checkpoint molecule by JX-594. Several studies have evaluated the therapeutic efficacy of combining OVs and ICIs.[12] Although the scope of this study was limited to testing the therapeutic efficacy of JX-594 monotherapy, the combination therapy of JX-594 and ICIs could be more potently effective, as shown in a previous study.[6]

However, considering the therapeutic efficacy of JX-594 monotherapy, the need for combining ICIs requires reconsideration. Although some of the combination strategies have demonstrated benefits compared with monotherapy, we should not overlook that combination therapy might lead to overtreatment, sparing the unnecessary toxicity and financial burden in cases that would have shown equivalent benefits from monotherapy. ICIs risk causing immune-mediated adverse effects, such as skin rash, pruritus, pneumonitis, diarrhea and/or immune-mediated colitis, hepatitis, and problems in the endocrine system.[36] A recent review article by Schirrmacher reported that OVs exert profoundly lower side effects, including major adverse events (WHO grades 3–4), than did other systemic therapies in patients with cancer.[37] Therefore, considering the sufficient therapeutic effects of JX-594, its use as monotherapy should also be considered.

The major challenge of standardizing OV is the proper delivery of viruses to the tumor site and eliciting antitumor immunity. To achieve significant efficacy in patients with cancer, OVs need to be delivered intratumorally.[38] Low efficiencies of both viral delivery to the tumor tissues and viral replication throughout the entire tumor tissue remain a challenge. These properties severely restrict the magnitude of therapeutic efficacy. Another hurdle is that the TME is highly immunosuppressive, and most OVs may not be able to modulate this effectively into pro-antitumor immunity.[38] The intratumoral injection of mJX-594 obviously induces a local immune response.[17] However, whether the systemic delivery of JX-594 could induce changes in the TME both in the primary tumors and the lung metastatic sites was uncertain. In this study, we showed that the systemic injection of JX-594 was well-delivered to the primary tumor and lung metastatic sites. Interestingly, the tumoral level of JX-594 increased more in the lung metastatic sites compared with that in the primary tumors. Although the mechanism is unclear, we believe that this is due to

연세대학교
YONSEI UNIVERSITY

the characteristics of the vaccinia virus. OV has an inherent capability of selectively targeting tumors, which was intensified through viral thymidine kinase gene deletion that led to significant attenuation in normal tissues.[39] During the development of a metastatic orthotopic RCC murine model, bioluminescent imaging (BLI) showed that lung metastatic sites have higher BLI signal intensities than do primary tumors as the days pass after the injection, demonstrating that active cancer cells are more densely placed at the metastasis sites.[29] Although it is only a hypothesis, malignant tumors metastasize to escape to a friendlier environment where a higher payoff is initially possible.[40] If OVs are more reluctant to move to a friendlier environment for cancer cells as shown in our study, the value of the OVs will be much higher. Further studies are warranted to clarify this finding.

Sunitinib continues to be administered as the first-line therapeutic agent in mRCC.[41] The European Association of Urology Guidelines on RCC recommend that, in patients who cannot receive or tolerate immune checkpoint inhibition, monotherapies with sunitinib, pazopanib, and cabozantinib are alternative treatment options.[42] The NCCN Kidney Cancer Panel also lists sunitinib as a category 1 preferred option for the first-line treatment for mRCCs with good-risk features, while recommended as another option in mRCCs with poor- or intermediate-risk features.[43] Our study also showed the robust therapeutic efficacy of sunitinib in the IMDC favorable-risk group, especially in reducing primary tumor burden. Furthermore, since second-line sunitinib demonstrates clinical activity after the failure of frontline immunotherapy in patients with mRCC, the role of TKIs should be reconsidered in this era where immunotherapy replaces targeted therapy.[44]

While sunitinib is associated with a potent angiogenic activity, recent clinical studies have highlighted its immune-modulatory effects.[45,46] Lawson et al. reported that sunitinib augments the immunotherapeutic efficacy of reovirus.[45] Ongoing angiogenesis contributes to immune evasion through the induction of a highly immunosuppressive TME.[46] Therefore, the use of angiogenesis inhibitor sunitinib to promote leukocyte infiltration into the tumor is an effective strategy to improve oncolytic virotherapy, although some of the limitations have to be overcome due to the poor understanding of the interaction between immunity and the vasculature. Special considerations for scheduling, dosing, and sequencing between immunotherapy agents and anti-angiogenic agents should be made since they assert antitumor activities at different stages, and their spatial and temporal modes of action might

연세대학교
YONSEI UNIVERSITY

differ.[46]

As reported by Chon et al., the tumor vessel density also reduced after the mJX-594 treatment in our study.[17] Along with a previous study, we also demonstrated that JX-594 is a potent but transient tumor vessel disruptor. As previously mentioned, angiogenesis is an important immune evasion mechanism, and vessel disrupting effects might also contribute to tumor regression.[46]

In this study, we developed two models based on the IMDC risk criteria. Although many treatment agents exist, these agents are recommended based on the IMDC risk criteria, which were developed in the TKI era.[24] These criteria are outdated considering the advancements in mRCC treatment. Therefore, future studies are needed to optimize the treatment strategies using specific molecular biomarkers to facilitate the clinical decision-making process in immunotherapy era.[47]

In 2018, the TRAcking Cancer Evolution through therapy (TRACERx) renal consortium published articles comprising a study of the origin, evolution and routes to metastasis of ccRCCs.[48-50] We selected the target gene for this study according to the evolutionary lineage of the TRACERx renal cohort.[49] Recently, Bui and colleagues published the first meta-analysis of genomic data from ccRCC tumors, reporting the four most commonly mutated genes in ccRCC of *VHL, PBRM1, SETD2*, and *BAP1*, with a mutation prevalence of 64%, 36%, 20%, and 13%, respectively.[25] *VHL* is a tumor suppressor gene located on chromosome 3p and is associated with hypoxia-inducible factors which acts as a potent transcriptional proangiogenic factor in RCC carcinogenesis.[51] The three other most frequently mutated genes, *PBRM1, SETD2,* and *BAP1,* are also located on chromosome 3p and contribute to DNA repair and transcriptional activation.[25]

PBRM1 and *BAP1* mutations are reported to be mutually exclusive, where *BAP1*-mutant tumors were associated with worse survival and a higher Fuhrman grade than *PBRM1*-mutant tumors.[52,53] This finding was supported by the MSKCC cohort study, where *BAP1* mutations with associated with poor prognostic factors such as a higher T stage, higher nuclear grade, large tumor size, more necrosis, and the presence of metastatic disease at presentation.[54] Our previous study also supported this finding that *BAP1* expression levels were significantly decreased in aggressive T1 stage ccRCC compared to non-aggressive T1 stage ccRCC.[55] In this study, *BAP1* mutation tumor demonstrated the most rapid growth

연세대학교
YONSEI UNIVERSITY

rate compared to other mutations.

Furthermore, therapeutic response was most effective in *BAP1* mutation tumor even after adjusting the relative tumor growth rate. Although the exact mechanisms are not clearly defined, we believe that this is due to the action mechanism of OVs. Among the two main mechanisms that explain the therapeutic efficacy of OVs, OVs' potential for inhibiting protein synthesis of tumor cells and destroying infected tumor cells by self-replication is the probable pathways that could explain why *BAP1* mutation tumor was most effectively reduced by JX-594.[12] Since *BAP1* mutation RCC tumors grow fast, they require more metabolic products. This could result in more vulnerability to the JX-594. However, OVs other mechanisms of action which is by recruiting and activating tumor-infiltrating immune cells should be evaluated in the future studies. *BAP1* mutation might induce increased number or activity of the tumor-infiltrating immune cells.

Recently, Langbein et al. reported that *BAP1* maintains hypoxia-inducible factor (HIF)-dependent IFN-β induction to suppress tumor growth in ccRCC.[56] In this study, we demonstrated that *BAP1*-deificient cell line had decreased levels of IFN-β expression in the control treatment group while it was most dramatically recovered after JX-594. Our results indicate that JX-594 suppressed *BAP1*-deficient tumor growth through the HIF-dependent IFN-β induction, and reactivating this pathway may be a novel therapeutic strategy for treating ccRCC.

Our study has its strength in evaluating the therapeutic efficacy of systemic treatment of JX-594 through two different models based on the IMDC risk criteria. Moreover, we have demonstrated the dynamic changes of TME in both primary tumor and lung metastatic sites. However, we were not able to demonstrate the therapeutic efficacy of combination therapy with JX-594 and ICIs since it was not the original scope of this study. Future studies are planned to evaluate the therapeutic efficacy of combination therapy of JX-594 and ICIs in mRCC. Second, we have only evaluated the DCs for the innate immunity since the mechanism of OVs is associated with antigen presentation to DCs. However, since sunitinib is known to be associated with myeloid-derived suppressor cells (MDSCs) which have immunosuppressive and proangiogenic activities,[57] we are currently under investigation of the role of sunitinib in the immunotherapy era by including MDSCs in future studies. Lastly, this is the first study to elucidate the potential of *BAP1* as predictive

연세대학교
YONSEI UNIVERSITY

biomarker for JX-594 treatment and its underlying mechanisms.

V. CONCLUSION

The systemic injection of JX-594 dynamically remodeled the TMEs from those of cold to those of hot tumors and activated anti-cancer immunity, which suppressed both the primary tumors and the lung metastases in early- and advanced-stage mRCCs. Sunitinib has limited efficacy in early-stage mRCC, but its role in improving the immunotherapeutic outcomes should be further investigated. *BAP1* demonstrated its potential for predictive biomarker for JX-594 treatment. Our study is the first to provide the findings that JX-594 monotherapy could be considered as the treatment option for mRCC and *BAP1* could be used as the guidance for the use of JX-594 although future clinical studies are needed.

연세대학교
YONSEI UNIVERSITY

REFERENCES

1. Sun M, Thuret R, Abdollah F, et al. Age-adjusted incidence, mortality, and survival rates of stage-specific renal cell carcinoma in North America: a trend analysis. Eur Urol 2011;59:135-41.
2. Gupta K, Miller JD, Li JZ, Russel MW, Charbonneau C. Epidemiologic and socioeconomic burden of metastatic renal cell carcinoma (mRCC): A literature review. Cancer Treat Rev 2008;34:193-205.
3. Stewart GD, O'Mahony FC, Powles T, Riddick ACP, Harrison DJ, Faratian D. What can molecular pathology contribute to the management of renal cell carcinoma? Nat Rev Urol 2011;8:255-65.
4. Motzer RJ, Hutson TE, Tomczak P, et al. Sunitinib versus interferon alfa in metastatic renal-cell carcinoma. New Engl J Med 2007;356:115-24.
5. Topalian SL, Drake CG, Pardoll DM. Immune Checkpoint Blockade: A Common Denominator Approach to Cancer Therapy. Cancer Cell 2015;27:450-61.
6. Lee YS, Lee WS, Kim CW, et al. Oncolytic vaccinia virus reinvigorates peritoneal immunity and cooperates with immune checkpoint inhibitor to suppress peritoneal carcinomatosis in colon cancer. J Immunother Cancer 2020;8.
7. Motzer RJ, Tannir NM, McDermott DF, et al. Nivolumab plus Ipilimumab versus Sunitinib in Advanced Renal-Cell Carcinoma. New Engl J Med 2018;378:1277-90.
8. Numakura K, Muto Y, Naito S, et al. Outcomes of axitinib versus sunitinib as first-line therapy to patients with metastatic renal cell carcinoma in the immune-oncology era. Cancer Med-Us 2021;10:5839-46.
9. Hasanov E, Gao J, Tannir NM. The Immunotherapy Revolution in Kidney Cancer Treatment: Scientific Rationale and First-Generation Results. Cancer J 2020;26:419-31.
10. Rini BI, Plimack ER, Stus V, et al. Pembrolizumab plus Axitinib versus Sunitinib for Advanced Renal-Cell Carcinoma. N Engl J Med 2019;380:1116-27.
11. Motzer RJ, Penkov K, Haanen J, et al. Avelumab plus Axitinib versus Sunitinib for Advanced Renal-Cell Carcinoma. N Engl J Med 2019;380:1103-15.
12. Oh CM, Chon HJ, Kim C. Combination Immunotherapy Using Oncolytic Virus for the Treatment of Advanced Solid Tumors. Int J Mol Sci 2020;21.
13. Bejarano L, Jordao MJC, Joyce JA. Therapeutic Targeting of the Tumor Microenvironment. Cancer Discov 2021;11:933-59.
14. Shofolawe-Bakare OT, Stokes LD, Hossain M, Smith AE, Werfel TA. Immunostimulatory biomaterials to boost tumor immunogenicity. Biomater Sci 2020;8:5516-37.
15. Xiao B, Zhang L, Liu H, et al. Oncolytic Adenovirus CD55-Smad4 Suppresses Cell Proliferation, Metastasis, and Tumor Stemness in Colorectal Cancer by Regulating Wnt/beta-Catenin Signaling Pathway. Biomedicines 2020;8.
16. Heo J, Reid T, Ruo L, et al. Randomized dose-finding clinical trial of oncolytic immunotherapeutic vaccinia JX-594 in liver cancer. Nat Med 2013;19:329-36.
17. Chon HJ, Lee WS, Yang H, et al. Tumor Microenvironment Remodeling by

연세대학교
YONSEI UNIVERSITY

Intratumoral Oncolytic Vaccinia Virus Enhances the Efficacy of Immune-Checkpoint Blockade. Clin Cancer Res 2019;25:1612-23.
18. Cripe TP, Ngo MC, Geller JI, et al. Phase 1 study of intratumoral Pexa-Vec (JX-594), an oncolytic and immunotherapeutic vaccinia virus, in pediatric cancer patients. Mol Ther 2015;23:602-8.
19. Abou-Alfa GK, Galle PR, Chao Y, et al. PHOCUS: A phase 3 randomized, open-label study comparing the oncolytic immunotherapy Pexa-Vec followed by sorafenib (SOR) vs SOR in patients with advanced hepatocellular carcinoma (HCC) without prior systemic therapy. J Clin Oncol 2016;34.
20. Tippu Z, Au L, Turajlic S. Evolution of Renal Cell Carcinoma. Eur Urol Focus 2021;7:148-51.
21. Voss MH, Kuo F, Chen D, et al. Integrated biomarker analysis for 412 renal cell cancer (RCC) patients (pts) treated on the phase 3 COMPARZ trial: Correlating common mutation events in PBRM1 and BAP1 with angiogenesis expression signatures and outcomes on tyrosine kinase inhibitor (TKI) therapy. J Clin Oncol 2017;35.
22. McDermott DF, Huseni MA, Atkins MB, et al. Clinical activity and molecular correlates of response to atezolizumab alone or in combination with bevacizumab versus sunitinib in renal cell carcinoma (vol 24, pg 749, 2018). Nature Medicine 2018;24:1941-.
23. Braun DA, Ishii Y, Walsh AM, et al. Clinical Validation of PBRM1 Alterations as a Marker of Immune Checkpoint Inhibitor Response in Renal Cell Carcinoma. Jama Oncol 2019;5:1631-3.
24. Yoshida T, Ohe C, Ikeda J, et al. Eosinophilic features in clear cell renal cell carcinoma correlate with outcomes of immune checkpoint and angiogenesis blockade. J Immunother Cancer 2021;9.
25. Bui TO, Dao VT, Nguyen VT, Feugeas JP, Pamoukdjian F, Bousquet G. Genomics of Clear-cell Renal Cell Carcinoma: A Systematic Review and Meta-analysis. European Urology 2022;81:349-61.
26. Wolf MM, Kimryn Rathmell W, Beckermann KE. Modeling clear cell renal cell carcinoma and therapeutic implications. Oncogene 2020;39:3413-26.
27. Breitbach CJ, Arulanandam R, De Silva N, et al. Oncolytic Vaccinia Virus Disrupts Tumor-Associated Vasculature in Humans. Cancer Res 2013;73:1265-75.
28. Lun XQ, Chan J, Zhou HY, et al. Efficacy and Safety/Toxicity Study of Recombinant Vaccinia Virus JX-594 in Two Immunocompetent Animal Models of Glioma. Molecular Therapy 2010;18:1927-36.
29. Park JS, Lee ME, Kim SH, Jang WS, Ham WS. Development of a highly pulmonary metastatic orthotopic renal cell carcinoma murine model. Biol Open 2021;10.
30. Felix J, Savvides SN. Mechanisms of immunomodulation by mammalian and viral decoy receptors: insights from structures. Nat Rev Immunol 2017;17:112-29.
31. Martin NT, Bell JC. Oncolytic Virus Combination Therapy: Killing One Bird with Two Stones. Molecular Therapy 2018;26:1414-22.
32. Kaufman HL, Kohlhapp FJ, Zloza A. Oncolytic viruses: a new class of immunotherapy drugs. Nat Rev Drug Discov 2015;14:642-+.

연세대학교
YONSEI UNIVERSITY

33. Bartlett DL, Liu ZQ, Sathaiah M, et al. Oncolytic viruses as therapeutic cancer vaccines. Mol Cancer 2013;12.
34. Conry RM, Westbrook B, Mckee S, Norwood TG. Talimogene laherparepvec: First in class oncolytic virotherapy. Hum Vacc Immunother 2018;14:839-46.
35. Rha SM, J.; Oh, SY.; Kim, C.; Bae, WK.; Lee, HW.; Dillon, M. A phase Ib study of recombinant vaccinia virus in combination with immune checkpoint inhibition (ICI) in advanced renal cell carcinoma (RCC). American Association for Cancer Research (AACR), Philadelphia, PA, USA 2020;80.
36. Grimm MO, Bex A, De Santis M, et al. Safe Use of Immune Checkpoint Inhibitors in the Multidisciplinary Management of Urological Cancer: The European Association of Urology Position in 2019. European Urology 2019;76:368-80.
37. Schirrmacher V. Cancer Vaccines and Oncolytic Viruses Exert Profoundly Lower Side Effects in Cancer Patients than Other Systemic Therapies: A Comparative Analysis. Biomedicines 2020;8.
38. Guo ZS. Oncolytic Virus Immunotherapy: Showcasing Impressive Progress in Special Issue II. Biomedicines 2021;9.
39. Kim JH, Oh JY, Park BH, et al. Systemic armed oncolytic and immunologic therapy for cancer with JX-594, a targeted poxvirus expressing GM-CSF. Mol Ther 2006;14:361-70.
40. Laruelle A, Manini C, Inarra E, Lopez JI. Metastasis, an Example of Evolvability. Cancers (Basel) 2021;13.
41. Sekino Y, Takemoto K, Murata D, et al. CD44 Is Involved in Sunitinib Resistance and Poor Progression-free Survival After Sunitinib Treatment of Renal Cell Carcinoma. Anticancer Res 2021;41:4875-83.
42. Bedke J, Albiges L, Capitanio U, et al. The 2021 Updated European Association of Urology Guidelines on Renal Cell Carcinoma: Immune Checkpoint Inhibitor-based Combination Therapies for Treatment-naive Metastatic Clear-cell Renal Cell Carcinoma Are Standard of Care. Eur Urol 2021;80:393-7.
43. Motzer RJ, Jonasch E, Boyle S, et al. NCCN Guidelines Insights: Kidney Cancer, Version 1.2021. J Natl Compr Canc Netw 2020;18:1160-70.
44. Wells JC, Dudani S, Gan CL, et al. Clinical Effectiveness of Second-line Sunitinib Following Immuno-oncology Therapy in Patients with Metastatic Renal Cell Carcinoma: A Real-world Study. Clin Genitourin Cancer 2021;19:354-61.
45. Lawson KA, Mostafa AA, Shi ZQ, et al. Repurposing Sunitinib with Oncolytic Reovirus as a Novel Immunotherapeutic Strategy for Renal Cell Carcinoma. Clinical Cancer Research 2016;22:5839-50.
46. Huinen ZR, Huijbers EJM, van Beijnum JR, Nowak-Sliwinska P, Griffioen AW. Anti-angiogenic agents - overcoming tumour endothelial cell anergy and improving immunotherapy outcomes. Nat Rev Clin Oncol 2021;18:527-40.
47. Park JS, Lee ME, Jang WS, et al. The DEAD/DEAH Box Helicase, DDX11, Is Essential for the Survival of Advanced Clear Cell Renal Cell Carcinoma and Is a Determinant of PARP Inhibitor Sensitivity. Cancers 2021;13.

연세대학교
YONSEI UNIVERSITY

48. Turajlic S, Xu H, Litchfield K, et al. Tracking Cancer Evolution Reveals Constrained Routes to Metastases: TRACERx Renal. Cell 2018;173:581-+.
49. Turajlic S, Xu H, Litchfield K, et al. Deterministic Evolutionary Trajectories Influence Primary Tumor Growth: TRACERx Renal. Cell 2018;173:595-610 e11.
50. Mitchell TJ, Turajlic S, Rowan A, et al. Timing the Landmark Events in the Evolution of Clear Cell Renal Cell Cancer: TRACERx Renal. Cell 2018;173:611-+.
51. Semenza GL. HIF-1 mediates metabolic responses to intratumoral hypoxia and oncogenic mutations. J Clin Invest 2013;123:3664-71.
52. Kapur P, Pena-Llopis S, Christie A, et al. Effects on survival of BAP1 and PBRM1 mutations in sporadic clear-cell renal-cell carcinoma: a retrospective analysis with independent validation. Lancet Oncol 2013;14:159-67.
53. Pena-Llopis S, Vega-Rubin-de-Celis S, Liao A, et al. BAP1 loss defines a new class of renal cell carcinoma (vol 44, pg 751, 2012). Nat Genet 2012;44:1072-.
54. Hakimi AA, Ostrovnaya I, Reva B, et al. Adverse Outcomes in Clear Cell Renal Cell Carcinoma with Mutations of 3p21 Epigenetic Regulators BAP1 and SETD2: A Report by MSKCC and the KIRC TCGA Research Network. Clinical Cancer Research 2013;19:3259-67.
55. Park JS, Lee HJ, Cho NH, et al. Risk Prediction Tool for Aggressive Tumors in Clinical T1 Stage Clear Cell Renal Cell Carcinoma Using Molecular Biomarkers. Comput Struct Biotec 2019;17:371-7.
56. Langbein LE, El Hajjar R, He S, et al. BAP1 maintains HIF-dependent interferon beta induction to suppress tumor growth in clear cell renal cell carcinoma. Cancer Lett 2022;547:215885.
57. Finke J, Ko J, Rini B, Rayman P, Ireland J, Cohen P. MDSC as a mechanism of tumor escape from sunitinib mediated anti-angiogenic therapy. Int Immunopharmacol 2011;11:856-61.

연세대학교
YONSEI UNIVERSITY

ABSTRACT (IN KOREAN)

전이성 신세포암에서의 암살상 바이러스의 치료 반응 예측을 위한 바이오마커의 탐색

<지도교수 함 원 식>

연세대학교 대학원 의학과

장 원 식

면역관문억제제와 혈관생성억제제는 전이성 신장암의 일차 치료제로써 사용되고 있으나 그 효과는 일부 환자에게만 나타나는 제한점을 가지고 있다. 암살상 바이러스인 JX-594 (pexastimogene devacirepvec, Pexa-vec) 는 여러 전임상 및 임상연구에서 적은 독성을 보이면서도 항암효과가 있는 것으로 알려져 있다. 이에 전이성 신장암 마우스에 JX-594를 투여하여 치료 효과를 확인하고 신장암에서 빈번하게 발생하는 4가지 돌연변이 유전자 (*VHL*, *PBRM1*, *SETD2*, *BAP1*)에 따른 치료 효과의 차이를 확인함으로써 치료 반응 예측을 위한 바이오마커를 개발하고자 하였다.

전이성 신장암 마우스에 JX-594 와 혈관생성억제제인 sunitinib을 각각 투여했을 때 sunitinib 치료군은 초기 전이성 신장암에서는 원발암과 폐 전이 병변 모두에서 종양 크기의 감소를 보였으나 후기 전이성 신장암에서는 그렇지 않았다. 반면 JX-594 치료군은 초기 및 후기 전이성 신장암 모두에서 원발암과 폐 전이 병변의 크기 감소가 나타났다. 이는 JX-594 치료 군에서 종양 침윤 CD 4/8+ T 세포 및 수지상 세포를 증가시킴으로써 원발암 및 폐 전이 병변에서 종양 내 미세 환경의 리모델링 된 결과임을 확인할 수 있었다. 또한 각각 *VHL*, *PBRM1*, *SETD2*, *BAP1* 돌연변이가 있는 4종류의 세포주 유래 종양 이종 이식 (Cell line-derived tumor xenograft, CDX) 마우스에 JX-594 치료 시 *BAP1* 돌연변이 종양에서 다른 돌연변이 (*VHL*, *PBRM1*, *SETD2*) 종양에 비해 상대적 치료 반응 비율이 가장 높았다. 한편, Interferon beta (IFN-β) 발현은

연세대학교
YONSEI UNIVERSITY

BAP1 돌연변이 세포주에서 다른 돌연변이 세포주에 비해 유의하게 감소한 반면, JX-594 처리 이후에는 가장 높은 비율로 회복되었다.

본 연구는 JX-594 가 전이성 신장암에 대한 치료 옵션으로 고려될 수 있으며 *BAP1* 돌연변이는 JX-594 치료 반응을 예측할 수 있는 바이오마커로써의 가능성이 있음을 확인한 최초의 연구이다. 하지만 이를 뒷받침할 만한 임상 연구가 향후 필요할 것이다.

핵심되는 말 : 암살상 바이러스, 신장암, 종양 내 미세환경, 바이오마커